Peripheral glia and neurons jointly regulate activity-induced synaptic remodeling at the *Drosophila* neuromuscular junction

Yen-Ching Chang[1], Yi-Jheng Peng[1], Joo Yeun Lee[1,#a], and Karen T. Chang[1,2*]

1. Zilkha Neurogenetic Institute, Keck School of Medicine, University of Southern California, CA 90089

2. Dept. of Physiology & Neuroscience, Keck School of Medicine, University of Southern California, CA 90089.

[#a] Current address: Department of Ophthalmology, University of California San Francisco, CA 94143-0518

* Corresponding author E-mail: changkt@usc.edu (KTC)

ABSTRACT

In the nervous system, reliable communication depends on the ability of neurons to adaptively remodel their synaptic structure and function in response to changes in neuronal activity. While neurons are the main drivers of synaptic plasticity, glial cells are increasingly recognized for their roles as active modulators. However, the underlying molecular mechanisms remain unclear. Here, using *Drosophila* neuromuscular junction as a model system for a tripartite synapse, we show that peripheral glial cells collaborate with neurons at the NMJ to regulate activity-induced synaptic remodeling, in part through a protein called shriveled (Shv). Shv is an activator of integrin signaling previously shown to be released by neurons during intense stimulation at the fly NMJ to regulate activity-induced synaptic remodeling. We demonstrate that Shv is also present in peripheral glia, and glial Shv is both necessary and sufficient for synaptic remodeling. However, unlike neuronal Shv, glial Shv does not activate integrin signaling at the NMJ. Instead, it regulates synaptic plasticity in two ways: 1) maintaining the extracellular balance of neuronal Shv proteins to regulate integrin signaling, and 2) controlling ambient extracellular glutamate concentration to regulate postsynaptic glutamate receptor abundance. Loss of glial cells showed the same phenotype as loss of Shv in glia. Together, these results reveal that neurons and glial cells homeostatically regulate extracellular Shv protein levels to control activity-induced synaptic remodeling. Additionally, peripheral glia maintains postsynaptic glutamate receptor abundance and contribute to activity-induced synaptic remodeling by regulating ambient glutamate concentration at the fly NMJ.

Introduction

The nervous system is highly plastic, with the capacity to undergo dynamic alterations in structure and strength in response to changing stimuli and environments (Lamprecht and LeDoux, 2004; Citri and Malenka, 2008). This activity-induced synaptic remodeling process is highly conserved across species and plays crucial roles in circuit formation during development, as well as in stabilizing existing connections post-development. Synaptic remodeling represents a finely orchestrated process, with communications across both the pre- and post- synapses to allow the growth of new synapses, and the stabilization and strengthening of existing ones. While much of the research on synaptic plasticity has concentrated on interactions between presynaptic axon terminals and postsynaptic cells, most synapses are tripartite synapses, with glial cells as the third cell type (Araque and Navarrete, 2010). Beyond simply providing metabolic support, glial cells are increasingly recognized for their roles as active modulators of synaptic plasticity (Sancho et al., 2021). However, how glial cells and neurons collaborate to coordinate activity-induced synaptic remodeling are not well understood.

The *Drosophila* larval neuromuscular junction (NMJ) is a genetically tractable system and a tripartite glutamatergic synapse that serves as an excellent model system to investigate mechanisms underlying activity-induced synaptic remodeling by glial cells (Banerjee and Bhat, 2008; Freeman, 2015; Kim et al., 2020). The peripheral glial cells at the fly NMJ perform some of the key functions similar to mammalian glia, including controlling neuronal excitability and conduction velocity (Kottmeier et al., 2020; Rey et al., 2023), recycling of neurotransmitters (Rival et al., 2004; Danjo et al., 2011), and engulfing

and clearing debris during damage to allow the growth of new boutons (Fuentes-Medel et al., 2009). They also release proteins such as transforming growth factor (TGF-β) to support synaptic growth (Fuentes-Medel et al., 2012), TNF-α (eiger) to influence neuronal survival (Keller et al., 2011), Wingless to regulate GluR clustering (Kerr et al., 2014), and laminin to control animal locomotion (Petley-Ragan et al., 2016). However, the role of peripheral glia in regulating activity-induced stabilization and remodeling of the existing synapses at the NMJ remains unknown.

Previous studies on activity-induced synaptic remodeling at the fly NMJ demonstrated that neuronal activity leads to the enlargement of existing boutons, accompanied by increases in postsynaptic GluR abundance (Lee et al., 2017; Chang et al., 2024). Intense neuronal stimulation triggers the release of a protein called Shriveled (Shv) by presynaptic motoneurons, which activates βPS integrin bi-directionally to stimulate synaptic bouton enlargement and elevate GluR levels on the postsynaptic muscles (Lee et al., 2017). Consequently, *shv* mutants display defective post-tetanic potentiation (PTP), a form of functional synaptic plasticity similar to the early phase of long-term potentiation (LTP) seen in mammalian neurons. Here we demonstrate that the Shv protein is also expressed in glial cells and is released extracellularly by peripheral glial cells. Glial Shv not only regulates basal GluR clustering but is also required for activity-induced synaptic remodeling. We further demonstrate that while glial Shv is present extracellularly, it does not respond to neuronal activity nor does it activate integrin signaling, unlike Shv derived from neurons. Instead, glial Shv contributes to synaptic plasticity regulation by modulating the levels of Shv release from neurons and by controlling the levels of ambient glutamate concentration. Restoring ambient glutamate

concentration could correct basal GluR abundance and defective synaptic plasticity caused by the loss of glial cells. These results further reveal that regulation of ambient extracellular glutamate concentration by glia is an important mechanism contributing to synaptic plasticity regulation.

Results

Shv is expressed in peripheral glia

To determine the role of Shv in glia, we first monitored its presence in different cell types. To this end, we knocked-in eGFP to the 3'-end of the full-length Shv protein using CRISPR/Cas9-catalyzed homology directed repair (Gratz et al., 2014). Western blots confirmed that the Shv protein is tagged with eGFP (Fig 1A), and immunostaining revealed its presence in neurons and glial cells (Fig 1B). Glial cells were identified using antibody against reverse polarity (Repo), a transcription factor expressed exclusively in glial cells (Xiong et al., 1994), and neuronal cells were marked either by Elav, a transcription factor expressed in neurons (Robinow and White, 1991), or HRP, which stains the neuronal cell membrane. We found that Shv-eGFP is present in both Repo and Elav positive cells in the larval brain, consistent with our previous report (Lee et al., 2017). Furthermore, Shv-eGFP can be detected at the NMJ, with weak signals in postsynaptic muscles and synaptic boutons, and stronger signals in peripheral glia (Fig 1C).

Glial Shv is required for activity-induced synaptic remodeling

Loss of Shv in *shv*^{1} mutant was previously shown to be essential for activity-induced synaptic remodeling (Lee et al., 2017). Given that Shv is observed in neurons,

glia, and muscle (Fig 1C), we determined the tissue-specific requirement for Shv by systematically knocking down *shv* using RNAi and tissue-specific drivers (Fig 2A). We found that *shv* knockdown in neurons using the pan-neuronal driver, *elav-GAL4,* generated the same phenotype as shv^1 mutant (Lee et al., 2017), namely smaller bouton size, reduced basal GluR intensity, and defective synaptic remodeling in response to neuronal stimulation. However, knockdown of *shv* in glia using the pan-glial specific driver, *repo-GAL4*, resulted in normal bouton size but significantly elevated GluR levels, as well as abolished activity-induced synaptic remodeling. This increase in GluR is unexpected and further suggests that neuronal and glial Shv acts through different pathways to regulate GluR abundance. Lastly, knockdown of *shv* in post-synaptic muscles using the muscle specific driver *24B-GAL4* did not affect synaptic development or activity-induced synaptic changes. Collectively, these results are consistent with an earlier finding that Shv is predominantly released by neurons to maintain activity-induced synaptic remodeling (Lee et al., 2017), as well as reveal an unexpected requirement for glial Shv in sustaining activity-induced synaptic changes and basal GluR abundance.

Given that reducing Shv in glia altered basal GluR levels during development, we used the GeneSwitch system to determine the temporal requirement for Shv in glia (Fig 2B). In the presence of RU486, the *repo-GeneSwitch* driver can undergo a conformational change to activate gene expression in glia (Osterwalder et al., 2001; Roman et al., 2001; Artiushin et al., 2018). When the 3rd instar larvae were fed with RU486 to transiently drive *shv-RNAi* expression in glia, we observed defective synaptic remodeling and elevated GluR levels. These results suggest an acute requirement for the glial Shv protein in regulating synaptic plasticity and GluR abundance.

Next, we determined the spatial requirement for Shv in glial cells. The peripheral glia can be divided into three subtypes: wrapping glia (WG) is the innermost layer, wrapping and contacting the peripheral nerve bundle; the subperineurial glial (SPG) covers the WG, establishing the blood-brain barrier; the perineurial glia (PGs) is located on the outermost surface of the nerve that is also part of the blood-brain barrier (Awasaki et al., 2008; Stork et al., 2008; Brink et al., 2012; Freeman, 2015; Fernandes et al., 2024) (Fig 3A). Using GAL4 lines previously shown to drive expression in the specific glial subtypes (Stork et al., 2012), we found that reducing Shv in either SPG or PG was sufficient to block activity-induced synaptic remodeling (Fig 3B), phenocopying *shv* knockdown in all glial cells (Fig 2A). NMJs with *shv* knockdown in wrapping glia (*nrv-Gal4*) exhibited normal activity-induced synaptic remodeling (Fig 3B). We also tested whether the astrocyte-like glia located in the central nervous system also contributes by knocking down Shv using *alrm-GAL4* (Doherty et al., 2009). We observed normal activity-induced synaptic remodeling (Fig 3). Together, these results suggest that Shv in PG and SPG glia, both in contact with synaptic boutons, extending into the muscles, and are part of the blood-brain barrier, are crucial for Shv function in glia and for synaptic remodeling.

Glial expression of Shv is sufficient to rescue synaptic plasticity in *shv* mutants

While it has been demonstrated that Shv derived from neurons is sufficient to rescue shv^1 mutant in activity-induced synaptic remodeling (Lee et al., 2017), it is not known whether glial Shv can compensate for the loss of neuronal Shv. To test this, we expressed Shv (*UAS-Shv*) in shv^1 mutant using the *repo-GAL4* driver. Figure 4A shows that glial expression of Shv was sufficient to restore basal GluR intensity and activity-

induced synaptic remodeling but did not normalize bouton size. These data demonstrate that while neuronal Shv is necessary to regulate bouton size during development, Shv derived from glia is sufficient to maintain basal GluR levels and support activity-induced synaptic modifications.

In addition to structural rescue, we next tested whether glial Shv can rescue functional plasticity. Electrophysiological recordings showed *shv*^{1} mutants displayed reduced miniature excitatory potential (mEPSP) amplitude but normal evoked EPSP (Fig 4B), consistent with a previous report (Lee et al., 2017). Selective expression of *shv* in glia was sufficient to restore mEPSP amplitude, in line with the rescue in GluR levels. Glial-specific expression of *shv* also rescued post-tetanic potentiation (PTP), an activity-dependent plasticity in *Drosophila* that is functionally similar to the initial stages of long-term potentiation (LTP) (Fig 4C). Collectively, these results suggest that glial Shv is sufficient to support functional and structural plasticity.

Glial Shv does not activate integrin signaling

Shv was previously shown to be released by neurons to trigger synaptic remodeling through integrin activation (Lee et al., 2017); we thus asked whether glial Shv restores synaptic plasticity in *shv*^{1} mutants by activating integrin signaling similar to its neuronal counterpart. Figure 5A shows that glia can indeed release Shv, as glial expression of HA tagged Shv (driven by *repo-GAL4*) can be detected extracellularly when stained using non-permeabilizing conditions. Next, we determined the effects of glial Shv on integrin signaling by monitoring the levels of phosphorylated focal adhesion kinase (pFAK), as its levels strongly correlate with integrin activation (Mitra et al., 2005; Tsai et

al., 2008). To our surprise, glial expression of *shv* in *shv*^{1} mutant did not restore pFAK levels to normal (Fig 5B). Furthermore, *shv* knockdown in glial cells exhibited higher pFAK staining compared to the control (Fig 5C), a result that is opposite to what was observed with shv knockdown in neurons (Lee et al., 2017). *shv* overexpression in glia, although did not change basal pFAK levels, blocked the activity-induced pFAK increases normally seen in control (Fig 5C). Collectively, these results suggest that glial Shv does not activate integrin and appears to play an inhibitory role in activity-induced integrin activation.

To elucidate whether glial Shv directly inhibits activity-induced integrin activation, we monitored the amount of Shv released by glia during neuronal activity by expressing Shv-HA in either glia or neurons of *shv*^{1} and measured its extracellular levels. Fig 5D demonstrates that while stimulation significantly increased extracellular Shv released by neurons, the amount of extracellular Shv released by glial cells was reduced. These data indicate that glial Shv does not directly inhibit integrin signaling. Next, we tested the hypothesis that glial Shv instead influences integrin signaling by regulating Shv release from neurons. To this end, we monitored Shv released by neurons or glia using the endogenously tagged Shv-eGFP line and tissue-specific knockdown of *shv*. When Shv was selectively knocked down in glia, an increase in extracellular Shv-eGFP level was observed at the NMJ (Fig 5E), which likely originated from neurons. This finding is consistent with a role for glial Shv in suppressing neuronal Shv release and further explains the higher pFAK level observed in case of glial *shv* knockdown (Fig 5C). A similar compensatory upregulation from glia was obtained when Shv was knocked down in neurons (Fig 5E). We also monitored the levels of Shv-eGFP in the larval brain, confirming that the *shv-RNAi* approach successfully reduced Shv levels in the selective cell types

(Sup Fig 1). Taken together, these results reveal that the amount of Shv released by neurons is homeostatically regulated by Shv produced in glia. Furthermore, unlike neurons, glial Shv release is independent of neuronal activity and does not directly alter integrin signaling.

Drosophila peripheral glia and Shv control ambient extracellular glutamate levels to regulate activity-induced synaptic remodeling

If Shv derived from glia does not activate integrin signaling, how does it restore synaptic plasticity in *shv*^{1}? One plausible explanation is that glial Shv is required for normal glial growth or survival. We therefore monitored glial morphology when Shv is knocked down in glia by co-expressing membrane targeted *CD4-tdGFP* using the *repo-GAL4* driver. Sup Fig 2 shows that there is no observable change in gross glial morphology, with glial processes extending and associating with proximal synaptic boutons, indicating glial Shv is not required for glial maintenance. This finding further bolster support for the claim that glial Shv does not activate integrin, which is essential for maintaining the integrity of peripheral glial layers (Xie and Auld, 2011).

An alternate possibility is that Shv modulates glial function to rescue activity-induced synaptic remodeling. Glial cells have an established role in providing support and maintaining glutamate homeostasis in the nervous system (Augustin et al., 2007). The *Drosophila* larval NMJ is a glutamatergic synapse with high ambient glutamate concentration in the hemolymph, with an average in the range of 1-2 mM glutamate (Chen et al., 2009). Surprisingly, the larval NMJ does not contain the excitatory amino acid transporter 1 protein (Eaat1), which is essential for removing extracellular glutamate,

suggesting that high extracellular glutamate is better tolerated and removed by diffusion through the hemolymph (Rival et al., 2006; Chen et al., 2009). The high ambient glutamate concentration is maintained by the cystine/glutamate antiporter (Cx-T), which imports cystine and exports glutamate into the extracellular milieu (Augustin et al., 2007; Grosjean et al., 2008). The purpose of the high extracellular glutamate is not well understood, but it is thought to control GluR clustering and maintain a reserved pool of GluR intracellularly (Chen et al., 2009). Given that we observed significantly upregulated GluR clustering when Shv was reduced in glia, we hypothesized that glial Shv may influence the levels of ambient extracellular glutamate. To detect glutamate level at the synapse, we took advantage of the GAL4/UAS and LexA/LexAop systems to express the glutamate sensor (iGluSnFR) in neurons while simultaneously knocking down or upregulating Shv in glia (Marvin et al., 2013) (Fig 6A). Knockdown of Shv in glia significantly reduced iGluSnFR signal, whereas upregulating Shv increased it, suggesting that glial Shv critically controls ambient extracellular glutamate levels. As a control, we also expressed Shv in neurons using *Elav-LexA* (Fig 6A). We found neuronal expression of Shv did not alter iGluSnFR signal at the synapse, confirming that the change in ambient glutamate level is selectively caused by Shv from glia.

Next, we set out to determine whether the reduced extracellular ambient glutamate is responsible for the defective synaptic remodeling observed when Shv is depleted in glia. To this end, we incubated the NMJ with HL-3 solution containing 2 mM glutamate for 1 hour before stimulating the NMJ with high KCl. Strikingly, this treatment condition not only corrected basal GluR levels, but also fully rescued the activity-induced synaptic remodeling defect seen in glial knockdown of *shv* (Fig 6B). In contrast, incubating the

NMJ with 2 mM glutamate did not correct basal GluR or activity-induced synaptic remodeling defect when Shv is knocked down in neurons (sup Fig 3). These data are consistent with the iGluSnFR imaging results and further confirm that glial and neuronal Shv acts through distinct pathways to jointly regulate synaptic remodeling.

To further understand the function of glial cells in synaptic plasticity regulation, we ablated glia by using the inducible *repo-GeneSwitch* driver to express *reaper (rpr)* in early third instar larvae. This method allows us to examine the acute requirement for glia while avoiding lethality associated with chronic glial ablation. Following RU486 treatment for 24 hours, fragmentation of the glial cell membrane and a reduction in GFP intensity was observed (Fig 7A), indicating degeneration of glial cells. This is consistent with an earlier report demonstrating that Rpr expression is sufficient to induce apoptosis and trigger cell death (White et al., 1996). Fig 7B shows that glial ablation caused the same phenotype as *shv* knockdown in glial cells (Fig 2A), with elevated basal GluR levels and blocked activity-induced synaptic remodeling. We hypothesized that if a primary role of glial cells in synaptic plasticity regulation is to maintain ambient extracellular glutamate levels, similar to glial Shv, then correcting extracellular glutamate concentration should be sufficient to restore synaptic plasticity, even in the absence of functional glia. Strikingly, incubating NMJs with 2 mM glutamate not only restored basal GluR levels but also rescued activity-induced synaptic remodeling caused by glial ablation (Fig 7B, 7C). Together, these data confirm that the ability of peripheral glial cells to maintain high ambient extracellular glutamate concentrations at the NMJ is crucial for synaptic plasticity.

Discussion

In this study, we show that the peripheral glial cells at the *Drosophila* NMJ play an important role in regulating synaptic plasticity. We demonstrate that neurons and glia jointly orchestrate activity-induced synaptic remodeling at the NMJ, with Shv playing a pivotal role. While neurons release Shv in an activity-dependent manner to regulate synaptic remodeling through integrin signaling (Lee et al., 2017), release of Shv by peripheral glial cells does not rely on neuronal activity and does not activate integrin signaling (Fig 5A-C). Instead, glial Shv influences activity-induced synaptic remodeling by keeping the levels of Shv released by neurons in check (Fig 5D-F) and controlling ambient extracellular glutamate levels (Fig 7).

Our data suggest that one mechanism underlying activity-induced synaptic remodeling by glia is through indirect control of Shv release from neurons, thereby maintaining minimal integrin signaling under ambient conditions. We propose that this low baseline integrin signaling enables neurons to respond with high sensitivity to enhanced integrin activation by Shv release from neurons following neuronal activity, leading to rapid synaptic remodeling. Conversely, knocking down Shv in glia removes this suppression, resulting in increased Shv release from neurons, higher basal integrin signaling, GluR levels, and pathway saturation, thereby inhibiting activity-induced synaptic remodeling. Supporting this, overexpression of Shv in neurons elevated basal pFAK and abolished synaptic plasticity (Lee et al., 2017). These findings also raise several intriguing questions for future research, including how neurons and glia distinguish different sources of Shv, and how they sense and communicate this information to regulate extracellular Shv levels from different cells.

Another main function of glial Shv is to regulate ambient extracellular glutamate

concentration. We report that overexpression of *shv* elevated ambient glutamate levels at the synapse measured using a genetically encoded glutamate sensor, whereas knockdown of *shv* in glia reduced its level (Fig 6B). Furthermore, ablating glia recapitulated the phenotypes of *shv* knockdown in glia, and transiently restoring extracellular ambient glutamate concentration efficiently rescued synaptic plasticity. It has been shown that the *Drosophila* larval NMJ maintains a surprisingly high ambient extracellular glutamate concentration, with an average in the range of 1-2 mM (Augustin et al., 2007). How Shv regulates extracellular glutamate concentration remains to be explored, but a likely mechanism is by affecting the levels or functions of the cystine/glutamate (Cx-T), which imports cystine and exports glutamate into the extracellular matrix. While Shv has been shown to activate integrin, it encodes a homolog of the mammalian DNAJB11protein (Lee et al., 2016), which functions as a molecular chaperone vital for proper protein folding in the endoplasmic reticulum (Shen et al., 2002). Shv thus could potentially be required for the proper folding and the function of the Cx-T, which is located on glial cell membrane at the fly NMJ (Augustin et al., 2007; Grosjean et al., 2008). Aligned with this, mutations in Cx-T also resulted in elevated basal GluR levels at the fly NMJ (Augustin et al., 2007). Future studies examining the functional interactions between Cx-T and Shv will shed light on mechanisms for Shv-dependent regulation of ambient extracellular glutamate levels at the NMJ.

How does extracellular glutamate regulate GluR levels and synaptic plasticity? Changes in glutamate levels has been shown to directly impact neurotransmission, glutamate receptor activity, and influence GluR clustering by internalizing the desensitized GluR (Featherstone and Shippy, 2008; Chen et al., 2009; Yao et al., 2018). We have also

shown that basal GluR level is homeostatically regulated by extracellular glutamate concentration (Fig 7). It is plausible that a high extracellular glutamate concentration enables the NMJ to maintain a reserved pool of GluRs that can be readily mobilized to the surface upon neuronal activity. Additionally, activation of GluR and downstream signaling pathways could trigger local protein translation machineries to prime the synapses to respond rapidly to changes in neuronal activity. Future studies examining intracellular mechanisms controlling activity-induced GluR increases will lead to better insights on synaptic plasticity regulation.

Materials and Methods

Fly stocks

Flies were maintained at 25°C on a standard fly food consisting of cornmeal, yeast, sugar, and agar, under a 12-hour light/dark cycle unless otherwise specified. The following fly lines were obtained from the Bloomington Drosophila Stock Center at Indiana University (BDSC, stock numbers in parentheses), the Vienna Drosophila Resource Center and Drosophila Genomics Resource Center (VDRC, specified before stock number), or Kyoto stock center (Kyoto, stock number in parentheses): *repo-GAL4* (BDSC, 7415), *24B-GAL4* (BDSC, 1767), *elav-GAL4* (BDSC, 458), *nSyb-GAL4* (BDSC, 51635), *Gliotactin-GAL4* (BDSC, 9030), *Nrv- GAL4* (BDSC, 6800), *alrm-GAL4* (BDSC, 67032), TRiP-RNAi control (BDSC, 35788), *iGluSnFR* (BDSC, 59611), *UAS-CD4-tdGFP* (BDSC, 35836), *UAS-IVS-myr::tdTomato* (BDSC, 32221), *Elav-LexA* (BDSC, 52676), *UAS-shv-RNAi* (VDRC 108576), *PG-GAL4* (also known as *NP6293-GAL4*, Kyoto, 105188), and, *repo-GeneSwitch-GAL4* (Artiushin et al., 2018), repo-LexA (a gift from Dr. Henry Y. Sun), *UAS-*

Shv and *shv*[1] (Lee et al., 2017).

To visualize the endogenous levels of Shv, Shv with eGFP inserted into the 3'-end of the endogenous Shv gene (Shv-eGFP) was generate using the CRISPR/Cas9 genome editing, and homology directed repair (HDR) as described (Gratz et al., 2014). Briefly, a target Cas9 cleavage site in Shv was selected at the 3' end of Shv without obvious off-target sequence in the Drosophila genome using CRISPR optimum Target Finger. The sgRNA target sequence: 5'- GCCGGCGAGCACTTTTATTG was cloned into the pU6-BbsI-chiRNA vector (Addgene, #45946). The vector for HDR contains the 5' homology arm containing Shv genomic region (1000 base pairs at the 3' end of the Shv gene with the stop codon removed) plus eGFP sequence, and the 3' homology arm (1020 base pair downstream of the Cas9 cleavage site in the Shv gene region) was cloned into pHD-DsRed (Addgene, # 51434). Both cloned vectors were injected into fly stocks containing Cas9 (BDSC 55821) and positive genome editing screen by the presence of DsRed by BestGene Inc. Insertion was confirmed by sequencing and Western blots.

LexAop-Shv RNAi and LexAop-Shv fly lines were generated by subcloning Shv-RNAi hairpin sequence based on VDRC Shv-RNAi design or the coding regions of Shv which contains a V5 tag into the pJFRC19-13XLexAop2-IVS-myr::GFP vector (Addgene, 26224). Both lines were inserted into the X chromosome specific position by microinjecting the plasmid into a P{CaryP}attP18 fly line (BDSC, 32107).

RU486 feeding

repo-GeneSwitch embryos were collected in 3 hours windows and early 3rd instar larvae (48 hours after larval hatching), were fed with food containing 10 μM RU486 (1:1000, 10

mM stock) or 0.1% EtOH (vehicle control) for 24 hours before dissection (Gatto and Broadie, 2008).

Immunochemistry

Dissection and stimulation of the third-instar larvae fillets were done as described (Lee et al., 2017). Briefly, dissected NMJs were fixed for 3 minutes at room temperature (RT) with Boutin's fixative for GluR staining. For all other antibodies, 4% paraformaldehyde was used (25 minutes at RT). The fixed samples were subsequently washed with either 0.1% Triton X-100 in PBS (PBST) or with PBS alone for a detergent-free condition. The samples were then blocked with 5% normal goat serum in either PBST or PBS, as specified. Primary antibodies used were: Rabbit anti-pFAK, 1:250 (Invitrogen, 44-624G), Rabbit anit-HA,1:1000 (Sigma, H6908), Rabbit anti-GluRIIC, 1:1000 (Chang et al., 2024), Cy3/Alexa-647 conjugated anti-HRP, 1:100 for non-permeabilized staining or 1:250 for permeabilized staining (Jackson ImmunoResearch); rat anti-Elav, 1:500 (7E8A10, Developmental Studies Hybridoma Bank at the University of Iowa (DSHB)); mouse anti-Repo, 1:50 (8D12, DSHB); mouse anti-GFP, 1:100 (4C9, DSHB). The secondary antibodies used were Alexa Fluor 488 or 405 conjugated, diluted at 1:250 (Invitrogen). For experiments with glutamate incubation, dissected preps were incubated with 2mM Glutamate solution for 1hr or 10 min before performing stimulation protocol as indicated. Mock controls were treated the same way but without 2mM glutamate.

Imaging and image analysis

Images of synaptic boutons from muscle 6/7, A2 or A3 were taken using Olympus FV3000 confocal microscope at 60X with 1.6 zoom. Images showing expression patterns were taken at lower magnifications with either 10X or 60X objectives. To establish changes in bouton size and GluR level, mock controls (unstimulated larvae) were always dissected, immunostained, and imaged in parallel with stimulated genotypes for each experiment using the same conditions. Image analyses for GluRIIC, bouton size and extracellular staining of Shv and pFAK done using the same protocol as described (Lee et al., 2017).

Electrophysiology

Third-instar larvae were dissected and immersed in a modified HL-3 solution containing NaCl (70 mM), KCl (5 mM), MgCl2 (10 mM), sucrose (115 mM), HEPES (5 mM), trehalose (5 mM), and NaHCO3 (10 mM), at pH 7.2, with specified concentrations of $CaCl_2$ (0.25 or 0.5 mM). Current-clamp recordings were performed on muscle area 6 in abdominal segments A2 or A3, using suction electrodes to stimulate the severed ventral nerves with a 0.3 ms stimulus duration. The recording electrode, filled with 3 M KCl and having a resistance between 15 and 40 mΩ, was used to acquire data. Data with resting potentials more hyperpolarized than -60 mV were analyzed, while datasets were excluded if resting potentials deviated by more than 10 mV during recording or if there was a sudden drop in EPSP amplitude, indicating incomplete nerve function. The experimental setup included an Axopatch 200B Amplifier, a Digidata 1440A for digitization, and pClamp 10.3 software (Molecular Devices) for control. Data analysis was conducted using MiniAnalysis (Synaptosoft), Clampfit (Molecular Devices), and Microsoft Excel, with nonlinear summation applied to correct the average EPSP.

Western blot

Drosophila larval brain extract was obtained by homogenizing 6-10 larval brains collected on ice in RIPA buffer with EDTA (50 mM Tris-HCl, pH7.5, 1% NP-40, 0.5% NaDoc, 150 mM NaCl, 0.1% SDS, 10 mM EDTA, 50 mM NaF, 1 mM Na3VO4, 250 nM cycloporin A, protease inhibitor cocktail (Roche) using mortar and pestle. Protein homogenate was separated by 10% SDS-PAGE and transferred to nitrocellulose membranes. Primary antibodies were diluted in blocking solution as following: rabbit anti-Shv, 1:400 (Lee et al., 2017); Rabbit Anti-GFP,1:1000 (NOVUS, NB600-308), Anti-β-tubulin, 1:500 (E7, DSHB).

Statistical Analysis

All data are shown as mean ± SEM. Sample sizes, indicated in the graphs or figure legends, represent biological replicates and adhere to established standards in the literature. Comparisons between unstimulated and stimulated samples of the paired genotype were made using Student's t-test. For comparisons involving multiple samples, one-way ANOVA followed by Tukey's multiple comparison test was employed to determine statistical significance. To minimize bias, all samples were randomized during dissection, image collection, and data analysis.

Acknowledgement

We would like to thank Dr. Amita Seghal and Dr. Henry Y. Sun for the generous gift of *repo-GeneSwitch-GAL4* and *repo-LexA*, respectively. K.T.C. is supported by NIH grants R01NS102260 and R01NS080946.

Author contributions

Y-C.C. performed most of the experiments and data analyses. Y-J.P. performed the electrophysiology experiments. J.Y.L. designed and helped to generate the Shv-eGFP line using CRISPR/Cas9, K.T.C. conceived, designed, and supervised all aspects of the project. Y-C.C. and K.T.C. wrote the manuscript with inputs from Y-J.P. All authors reviewed and edited the manuscript.

Competing Interest

The authors declare no competing interests.

Data Availability

Additional information and requests for reagents used in this study are available upon request.

Reference

Araque A, Navarrete M (2010) Glial cells in neuronal network function. Philos Trans R Soc Lond B Biol Sci 365:2375-2381.

Artiushin G, Zhang SL, Tricoire H, Sehgal A (2018) Endocytosis at the Drosophila blood-brain barrier as a function for sleep. Elife 7.

Augustin H, Grosjean Y, Chen K, Sheng Q, Featherstone DE (2007) Nonvesicular release of glutamate by glial xCT transporters suppresses glutamate receptor clustering in vivo. J Neurosci 27:111-123.

Awasaki T, Lai SL, Ito K, Lee T (2008) Organization and postembryonic development of glial cells in the adult central brain of Drosophila. J Neurosci 28:13742-13753.

Banerjee S, Bhat MA (2008) Glial ensheathment of peripheral axons in Drosophila. J Neurosci Res 86:1189-1198.

Brink DL, Gilbert M, Xie X, Petley-Ragan L, Auld VJ (2012) Glial processes at the Drosophila larval neuromuscular junction match synaptic growth. PloS one 7:e37876.

Chang YC, Gao Y, Lee JY, Peng YJ, Langen J, Chang KT (2024) Identification of secretory autophagy as a mechanism modulating activity-induced synaptic remodeling. Proc Natl Acad Sci U S A 121:e2315958121.

Chen K, Augustin H, Featherstone DE (2009) Effect of ambient extracellular glutamate on Drosophila glutamate receptor trafficking and function. J Comp Physiol A Neuroethol Sens Neural Behav Physiol 195:21-29.

Citri A, Malenka RC (2008) Synaptic plasticity: multiple forms, functions, and mechanisms. Neuropsychopharmacology 33:18-41.

Danjo R, Kawasaki F, Ordway RW (2011) A tripartite synapse model in Drosophila. PloS one 6:e17131.

Doherty J, Logan MA, Tasdemir OE, Freeman MR (2009) Ensheathing glia function as phagocytes in the adult Drosophila brain. J Neurosci 29:4768-4781.

Featherstone DE, Shippy SA (2008) Regulation of synaptic transmission by ambient extracellular glutamate. The Neuroscientist : a review journal bringing neurobiology, neurology and psychiatry 14:171-181.

Fernandes VM, Auld V, Klambt C (2024) Glia as Functional Barriers and Signaling Intermediaries. Cold Spring Harb Perspect Biol 16.

Freeman MR (2015) Drosophila Central Nervous System Glia. Cold Spring Harb Perspect Biol 7.

Fuentes-Medel Y, Logan MA, Ashley J, Ataman B, Budnik V, Freeman MR (2009) Glia and muscle sculpt neuromuscular arbors by engulfing destabilized synaptic boutons and shed presynaptic debris. PLoS Biol 7:e1000184.

Fuentes-Medel Y, Ashley J, Barria R, Maloney R, Freeman M, Budnik V (2012) Integration of a retrograde signal during synapse formation by glia-secreted TGF-beta ligand. Current biology : CB 22:1831-1838.

Gatto CL, Broadie K (2008) Temporal requirements of the fragile X mental retardation protein in the regulation of synaptic structure. Development 135:2637-2648.

Gratz SJ, Ukken FP, Rubinstein CD, Thiede G, Donohue LK, Cummings AM, O'Connor-Giles KM (2014) Highly specific and efficient CRISPR/Cas9-catalyzed homology-directed repair in Drosophila. Genetics 196:961-971.

Grosjean Y, Grillet M, Augustin H, Ferveur JF, Featherstone DE (2008) A glial amino-acid transporter controls synapse strength and courtship in Drosophila. Nat Neurosci 11:54-61.

Keller LC, Cheng L, Locke CJ, Muller M, Fetter RD, Davis GW (2011) Glial-derived prodegenerative signaling in the Drosophila neuromuscular system. Neuron 72:760-775.

Kerr KS, Fuentes-Medel Y, Brewer C, Barria R, Ashley J, Abruzzi KC, Sheehan A, Tasdemir-Yilmaz OE, Freeman MR, Budnik V (2014) Glial wingless/Wnt regulates glutamate receptor clustering and synaptic physiology at the Drosophila neuromuscular junction. J Neurosci 34:2910-2920.

Kim T, Song B, Lee IS (2020) Drosophila Glia: Models for Human Neurodevelopmental and Neurodegenerative Disorders. Int J Mol Sci 21.

Kottmeier R, Bittern J, Schoofs A, Scheiwe F, Matzat T, Pankratz M, Klambt C (2020) Wrapping glia regulates neuronal signaling speed and precision in the peripheral nervous system of Drosophila. Nat Commun 11:4491.

Lamprecht R, LeDoux J (2004) Structural plasticity and memory. Nat Rev Neurosci 5:45-54.
Lee JY, Chen JY, Shaw JL, Chang KT (2016) Maintenance of Stem Cell Niche Integrity by a Novel Activator of Integrin Signaling. PLoS Genet 12:e1006043.
Lee JY, Geng J, Lee J, Wang AR, Chang KT (2017) Activity-Induced Synaptic Structural Modifications by an Activator of Integrin Signaling at the. J Neurosci 37:3246-3263.
Marvin JS, Borghuis BG, Tian L, Cichon J, Harnett MT, Akerboom J, Gordus A, Renninger SL, Chen TW, Bargmann CI, Orger MB, Schreiter ER, Demb JB, Gan WB, Hires SA, Looger LL (2013) An optimized fluorescent probe for visualizing glutamate neurotransmission. Nat Methods 10:162-170.
Mitra SK, Hanson DA, Schlaepfer DD (2005) Focal adhesion kinase: in command and control of cell motility. Nat Rev Mol Cell Biol 6:56-68.
Osterwalder T, Yoon KS, White BH, Keshishian H (2001) A conditional tissue-specific transgene expression system using inducible GAL4. Proc Natl Acad Sci U S A 98:12596-12601.
Petley-Ragan LM, Ardiel EL, Rankin CH, Auld VJ (2016) Accumulation of Laminin Monomers in Drosophila Glia Leads to Glial Endoplasmic Reticulum Stress and Disrupted Larval Locomotion. J Neurosci 36:1151-1164.
Rey S, Ohm H, Moschref F, Zeuschner D, Praetz M, Klambt C (2023) Glial-dependent clustering of voltage-gated ion channels in Drosophila precedes myelin formation. Elife 12.
Rival T, Soustelle L, Strambi C, Besson MT, Iche M, Birman S (2004) Decreasing glutamate buffering capacity triggers oxidative stress and neuropil degeneration in the Drosophila brain. Current biology : CB 14:599-605.
Rival T, Soustelle L, Cattaert D, Strambi C, Iche M, Birman S (2006) Physiological requirement for the glutamate transporter dEAAT1 at the adult Drosophila neuromuscular junction. J Neurobiol 66:1061-1074.
Robinow S, White K (1991) Characterization and spatial distribution of the ELAV protein during Drosophila melanogaster development. J Neurobiol 22:443-461.
Roman G, Endo K, Zong L, Davis RL (2001) P[Switch], a system for spatial and temporal control of gene expression in Drosophila melanogaster. Proc Natl Acad Sci U S A 98:12602-12607.
Sancho L, Contreras M, Allen NJ (2021) Glia as sculptors of synaptic plasticity. Neurosci Res 167:17-29.
Shen Y, Meunier L, Hendershot LM (2002) Identification and characterization of a novel endoplasmic reticulum (ER) DnaJ homologue, which stimulates ATPase activity of BiP in vitro and is induced by ER stress. J Biol Chem 277:15947-15956.
Stork T, Bernardos R, Freeman MR (2012) Analysis of glial cell development and function in Drosophila. Cold Spring Harb Protoc 2012:1-17.
Stork T, Engelen D, Krudewig A, Silies M, Bainton RJ, Klambt C (2008) Organization and function of the blood-brain barrier in Drosophila. J Neurosci 28:587-597.
Tsai PI, Kao HH, Grabbe C, Lee YT, Ghose A, Lai TT, Peng KP, Van Vactor D, Palmer RH, Chen RH, Yeh SR, Chien CT (2008) Fak56 functions downstream of integrin alphaPS3betanu and suppresses MAPK activation in neuromuscular junction growth. Neural Dev 3:26.

White K, Tahaoglu E, Steller H (1996) Cell killing by the Drosophila gene reaper. Science 271:805-807.
Xie X, Auld VJ (2011) Integrins are necessary for the development and maintenance of the glial layers in the Drosophila peripheral nerve. Development 138:3813-3822.
Xiong WC, Okano H, Patel NH, Blendy JA, Montell C (1994) repo encodes a glial-specific homeo domain protein required in the Drosophila nervous system. Genes Dev 8:981-994.
Yao L, Grand T, Hanson JE, Paoletti P, Zhou Q (2018) Higher ambient synaptic glutamate at inhibitory versus excitatory neurons differentially impacts NMDA receptor activity. Nat Commun 9:4000.

Figure legends

Figure 1. Endogenous Shv tagged with eGFP is detected in glial cells. (A) Schematic of eGFP knock-in to the Shv gene generated using CRISPR/Cas9 system (top). Exons are in orange, signal peptide in red. Western blots using antibodies against GFP and Shv confirms the presence of eGFP in Shv. β-tubulin is used as a loading control. **(B)** Low magnification images of the 3rd instar larval brain showing weak Shv-eGFP signal throughout the brain (left). Scale bar = 100 μM. Zoomed in view of the brain hemisphere and ventral nerve cord with neurons and glia marked by Elav and Repo antibodies, respectively. Asterisks label glial cells with Shv expression. Scale bar for brain and VNC are 10 and 15 μM, respectively. **(C)** Shv-eGFP can be detected at the NMJ. Glial membrane is marked by membrane targeted tdTomato (driven by glial specific Repo-GAL4) and neuronal membrane labeled by HRP. Zoomed in views show that Shv-eGFP colocalizes with glial membrane (magenta arrow) and synaptic boutons (yellow arrow).

Shv-eGFP also weakly labels the muscle. Scale bar = 10 μM in the upper panels, and 2 μM in the lower panels.

Figure 2. Shv in glia is necessary for activity-induced synaptic remodeling. (A) Tissue-specific knockdown of *shv*. Reducing Shv in neurons or glia blocks activity-induced synaptic remodeling, but not when *shv* is knocked down in muscles. Notably, glia-specific knockdown of *shv* increases the levels of GluRIIC, whereas neuronal Shv knockdown decreases basal GluRIIC. **(B)** Acute knockdown of *shv* in glia using the inducible *repo-GeneSwitch-GAL4* driver affects basal GluR intensity and abolishes activity-induced synaptic changes. (A) and (B), Scale bar = 2 μm. All values are normalized to unstimulated control and presented as mean ± S.E.M. Control contains TRiP RNAi control vector driven by the indicated driver. Statistics: One-way Anova followed by Tukey's multiple comparison test was used to compare between unstimulated control and unstimulated NMJs across genotypes. Student's t-test was used to compare between unstimulated and stimulated NMJs of the same genotype. # $p \leq 0.05$; ## $p \leq 0.01$; ### $p \leq 0.001$ when comparing unstimulated samples to unstimulated control. *$p \leq 0.05$; **$p \leq 0.01$; ***$p \leq 0.001$ when comparing stimulated to unstimulated NMJs.

Figure 3. Expression of shv in perineurial and subperineurial glia is required for activity-induced synaptic remodeling. (A) Diagram of relative membrane position and extension of WG, SPG, and PG at the NMJ. Astrocyte-like glia can be detected in the central brain and ventral nerve chord. **(B)** Representative images and quantification of synaptic changes following knockdown of *shv* in glia subtypes. Knockdown of *shv* in SPG and PG recapitulate the phenotypes of pan-neuronal knockdown, as well as abolish

activity-induced synaptic remodeling. Scale bar = 2 μm. All values are normalized to unstimulated control and presented as mean ± S.E.M. Control contains TRiP RNAi control vector driven by the indicated driver. Statistics: One-way Anova followed by Tukey's multiple comparison test was used to compare between unstimulated control and unstimulated NMJs across genotypes. Student's t-test was used to compare between unstimulated and stimulated NMJs of the same genotype. # $p \leq 0.05$; ### $p \leq 0.001$ when comparing unstimulated samples to unstimulated control. *$p \leq 0.05$; **$p \leq 0.01$; ***$p \leq 0.001$ when comparing stimulated to unstimulated NMJs.

Figure 4. Glial Shv rescues defective synaptic plasticity observed in *shv^1* mutant. **(A)** Selective expression of *shv* in glia of *shv^1* mutants is sufficient to rescue activity-dependent synaptic changes but not basal bouton size. Scale bar = 2μm. **(B)** Representative mEPSP and eEPSP recordings conducted using HL3 solution containing 0.5 mM Ca^{2+}. Average eEPSP amplitude is shown after nonlinear summation correction. **(C)** Normalized eEPSP before and following tetanus (10 Hz for 2 min) at the indicated time points. Recordings were done using HL3 solution containing 0.25 mM Ca^{2+}. *shv^1* showed significantly diminished PTP following stimulation. Expression of *shv* in glial cells of *shv^1* rescued PTP. The number of NMJs examined is shown in parentheses. Student's t-test was used to compare between control and the indicated genotypes. * shows that *shv^1* displays PTP that is significantly lower than the control ($p \leq 0.05$), starting from the indicated time and onwards. All values are mean ± S.E.M. For (A) and (B), one-way Anova followed by Tukey's multiple comparison test was used to compare between unstimulated control and unstimulated NMJs across genotypes. Student's t-test was used to compare

between unstimulated and stimulated NMJs of the same genotype. # $p \leq 0.05$; ## $p \leq 0.01$; ### $p \leq 0.001$ when comparing unstimulated samples to unstimulated control. *$p \leq 0.05$; **$p \leq 0.01$ when comparing stimulated to unstimulated NMJs.

Figure 5. Glial Shv does not activate integrin signaling but modulates neuronal release of Shv. (A) Representative images showing that Shv can be detected extracellularly when expressed using glial-specific driver. Extracellular Shv-HA (Shv^{extra})is monitored using an antibody against HA under detergent-free staining condition. **(B)** Expression of Shv using the glial-specific driver does not rescue pFAK levels during unstimulated and stimulated conditions, revealing that glial Shv does not activate integrin. **(C)** Knockdown of *shv* in glia upregulated pFAK, whereas upregulation of *shv* in glia blocked the activity-dependent increase normally seen in control. **(D)** Expression of *shv* in shv^{1} mutants show activity-dependent release of Shv by neurons, but not by glia. Shv^{extra} indicates extracellular Shv stained using detergent-free conditions. **(E)** Knockdown of endogenous Shv-eGFP in neurons or glia did not diminish extracellular presence of Shv-eGFP at the NMJ, suggesting homeostatic regulation of Shv protein level. Scale bar = 2 μm for all panels. All values are normalized to unstimulated control and presented as mean ± S.E.M. One-way Anova followed by Tukey's multiple comparison test was used to compare between unstimulated control and unstimulated NMJs across genotypes. Student's t-test was used to compare between unstimulated and stimulated NMJs of the same genotype. # $p \leq 0.05$; ** $p \leq 0.01$; ### $p \leq 0.001$ when comparing unstimulated samples to unstimulated control. *$p \leq 0.05$; **$p \leq 0.01$; ***$p \leq 0.001$ when comparing stimulated to unstimulated NMJs.

Figure 6. Glial Shv regulates ambient extracellular glutamate concentration. (A) Shv expression in glia maintains ambient glutamate concentration at the NMJ. Left panel shows a schematic of the tripartite synapse at the NMJ. iGluSnFR expression in neurons via the GAL4/UAS system can detect extracellular ambient glutamate concentration at the synapse, while glia-specific knockdown or upregulation of Shv is achieved using the LexA/LexAop system. iGluSnFR signals are seen in green and HRP-Cy3 was added to mark neuronal membrane (middle panels). Lower graph shows quantitation of the relative ambient glutamate concentration at the NMJ. Only Shv from glia affects ambient glutamate concentration, Shv from neurons does not. **(B)** Incubating the NMJ with 2 mM glutamate rescues synaptic remodeling in case of glial Shv knockdown. Vehicle controls represent NMJs dissected in parallel and incubated with HL3 without 2mM glutamate for the same length of time. Scale bar = 2μm. All values are normalized to unstimulated control and presented as mean ± S.E.M. Control contains TRiP RNAi control vector driven by the indicated driver. Statistics: One-way Anova followed by Tukey's multiple comparison test was used to compare between unstimulated control and unstimulated NMJs across genotypes. Student's t-test was used to compare between unstimulated and stimulated NMJs of the same genotype. # $p \leq 0.05$; ### $p \leq 0.001$ when comparing unstimulated samples to unstimulated control. *$p \leq 0.05$; **$p \leq 0.01$; ***$p \leq 0.001$ when comparing stimulated to unstimulated NMJs.

Figure 7. Acute ablation of glia elevated basal GluR levels and disrupted activity-induced synaptic remodeling, but extracellular glutamate incubation is sufficient

to compensate for the loss of glia. (A) Transient *rpr* expression is sufficient to trigger death of glial cells. Diagram shows the RU486 feeding protocol used to induce glial cell death in 3rd instar larvae. Lower panels show images of the segmental nerves (left) and the NMJ (middle). The zoomed in region of the NMJ (yellow box) is magnified on the right. Glial membrane is marked by CD4-tdGFP, which appears fragmented in the presence of rpr expression, indicating glial cell death. Scale bars indicate size in μm. **(B)** Images and **(C)** quantitation of synaptic bouton size and GluR abundance. Incubating the NMJ for 10 minutes with 2 mM glutamate is sufficient to overcome loss of glial cells and restore basal GluR level and activity-induced synaptic remodeling, suggesting a main function of peripheral glia in synaptic plasticity regulation is to maintain a high ambient glutamate concentration. Scale bar = 2μm in (B). All values are normalized to unstimulated control and presented as mean ± S.E.M. Control contains TRiP RNAi control vector driven by the indicated driver. Statistics: One-way Anova followed by Tukey's multiple comparison test was used to compare between unstimulated control and unstimulated NMJs across genotypes. Student's t-test was used to compare between unstimulated and stimulated NMJs of the same genotype. ### $p \leq 0.001$ when comparing unstimulated samples to unstimulated control. *$p \leq 0.05$; ***$p \leq 0.001$ when comparing stimulated to unstimulated NMJs.

List of Supplementary Materials

Supplementary Figure 1. Efficiency of *shv* knockdown by RNAi in neurons and glia.

Supplementary Figure 2. Integrity of peripheral glial cell membranes.

Supplementary Figure 3. Defective activity-induced synaptic remodeling caused by the loss of neuronal Shv is not rescued by incubation with 2 mM glutamate.

Figure 1

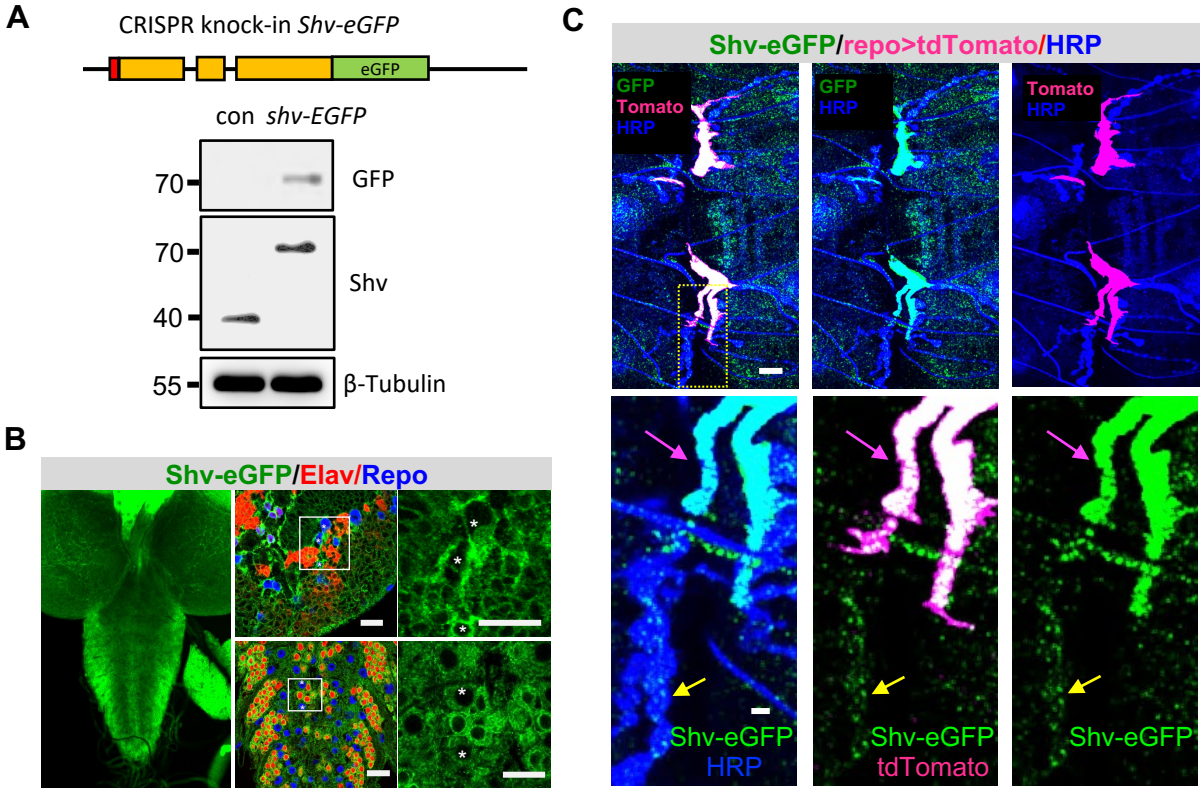
A
CRISPR knock-in Shv-eGFP
eGFP
con shv-EGFP
70
GFP
70
Shv
40
55
β-Tubulin
B
Shv-eGFP/Elav/Repo
C
Shv-eGFP/repo>tdTomato/HRP
GFP
Tomato
HRP
GFP
HRP
Tomato
HRP
Shv-eGFP
HRP
Shv-eGFP
tdTomato
Shv-eGFP

Figure 2

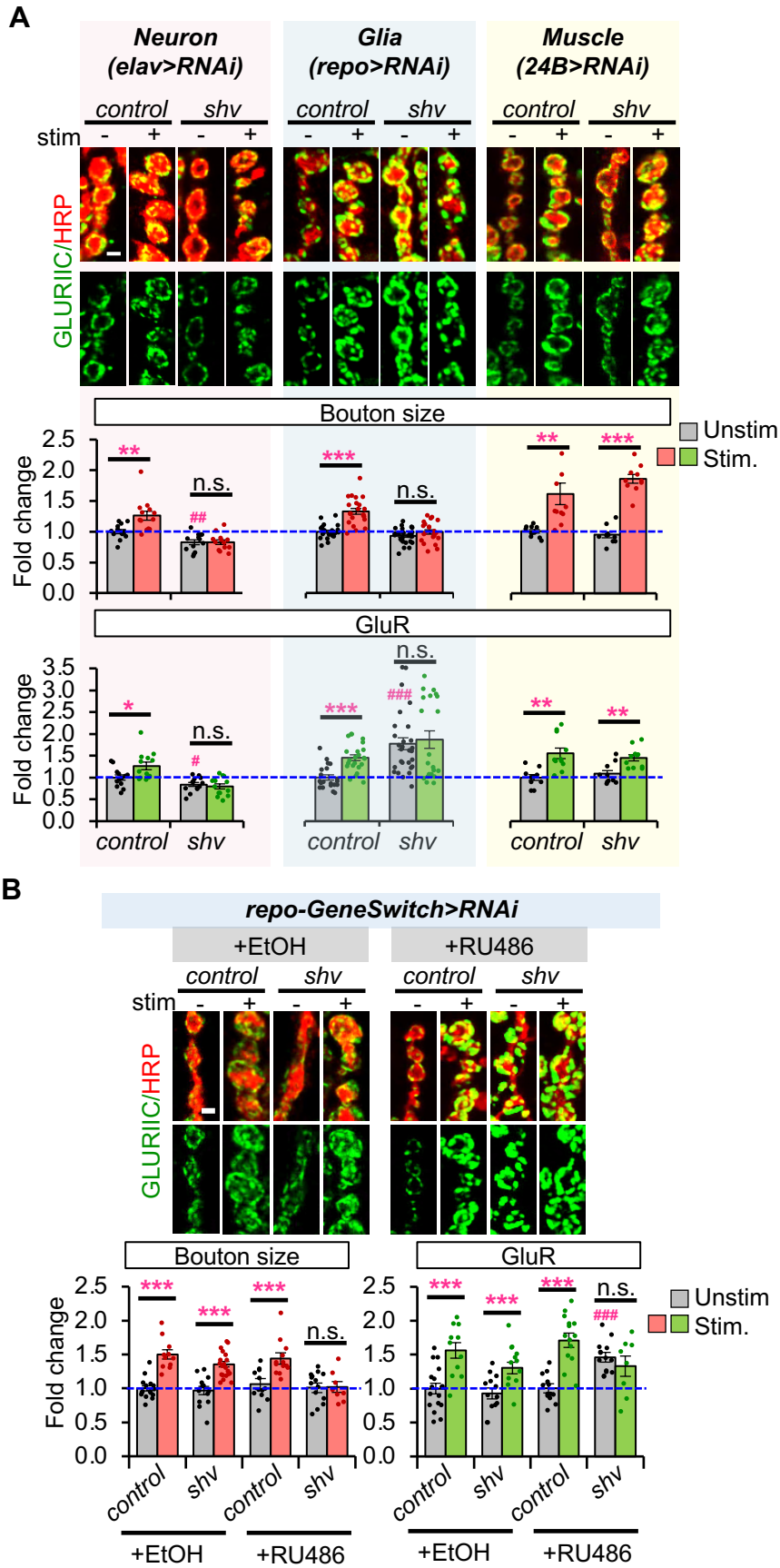
A
Neuron (elav>RNAi)
Glia (repo>RNAi)
Muscle (24B>RNAi)
control
shv
stim
GLURIIC/HRP
Bouton size
GluR
Fold change
Unstim
Stim.
n.s.
B
repo-GeneSwitch>RNAi
+EtOH
+RU486

Figure 3

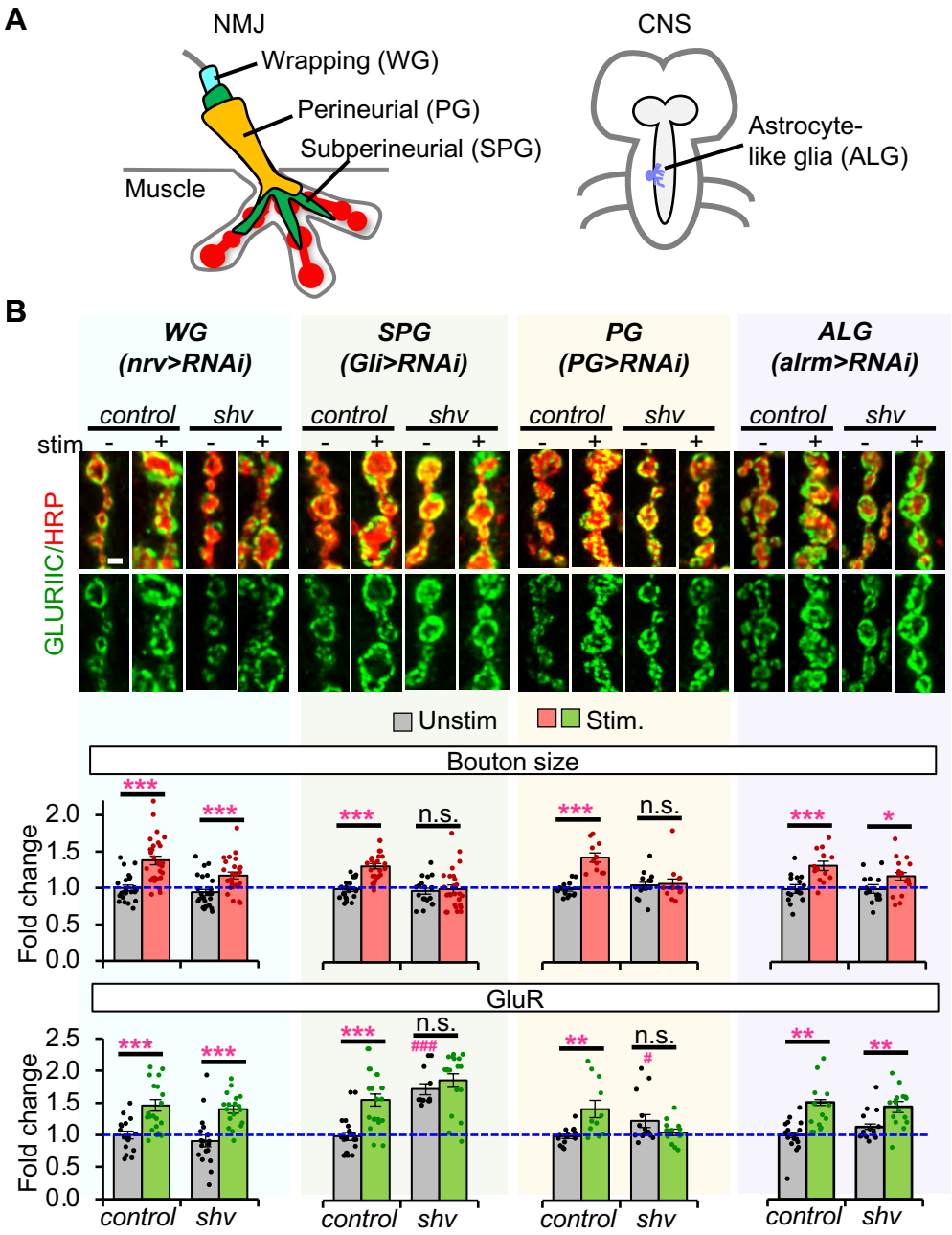
A
NMJ
Wrapping (WG)
Perineurial (PG)
Subperineurial (SPG)
Muscle
CNS
Astrocyte-like glia (ALG)
B
WG (nrv>RNAi)
SPG (Gli>RNAi)
PG (PG>RNAi)
ALG (alrm>RNAi)
control
shv
stim
GLURIIC/HRP
Unstim
Stim.
Bouton size
GluR
Fold change
n.s.

Figure 4

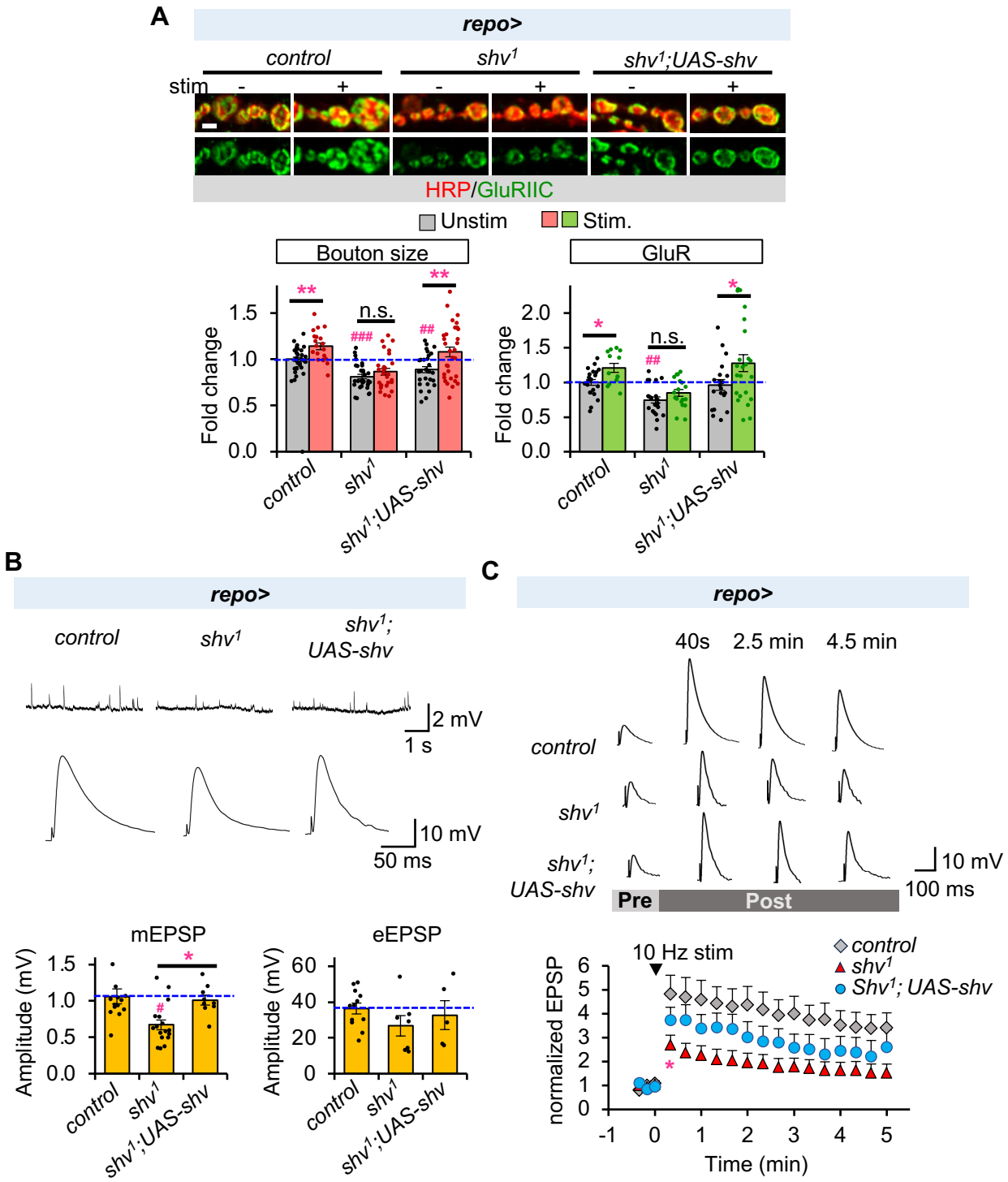
A
repo>
control
shv1
shv1;UAS-shv
stim
-
+
HRP/GluRIIC
Unstim
Stim.
Bouton size
GluR
Fold change
n.s.
control
shv1
shv1;UAS-shv
B
repo>
control
shv1
shv1; UAS-shv
2 mV
1 s
10 mV
50 ms
mEPSP
eEPSP
Amplitude (mV)
C
repo>
40s
2.5 min
4.5 min
control
shv1
shv1; UAS-shv
10 mV
100 ms
Pre
Post
10 Hz stim
control
shv1
Shv1; UAS-shv
normalized EPSP
Time (min)

Figure 5

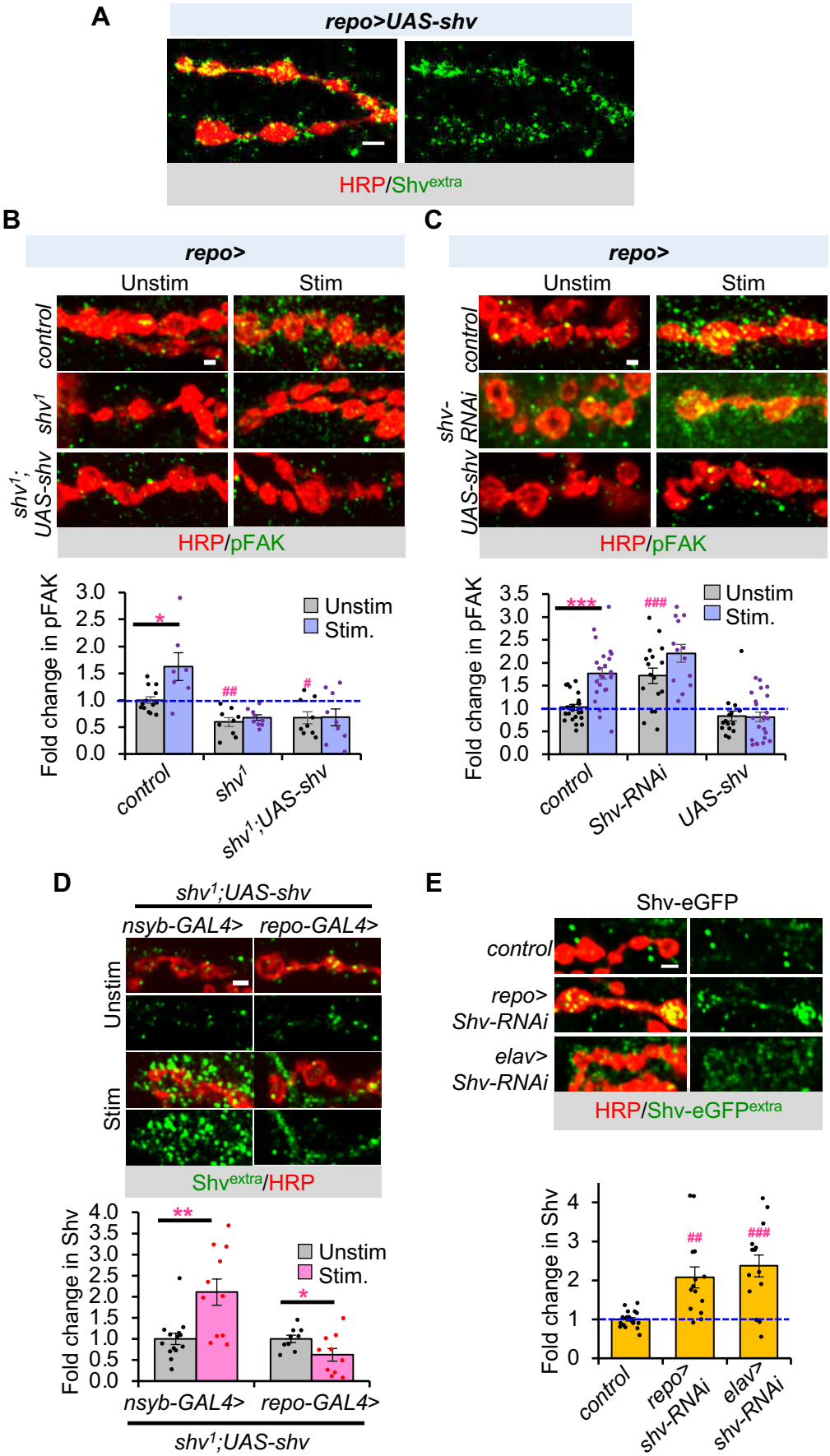
A
repo>UAS-shv
HRP/Shv^extra
B
repo>
Unstim
Stim
control
shv1
shv1; UAS-shv
HRP/pFAK
Fold change in pFAK
Unstim
Stim.
control
shv1
shv1;UAS-shv
C
repo>
Unstim
Stim
control
shv-RNAi
UAS-shv
HRP/pFAK
Fold change in pFAK
Unstim
Stim.
control
Shv-RNAi
UAS-shv
D
shv1;UAS-shv
nsyb-GAL4>
repo-GAL4>
Unstim
Stim
Shv^extra/HRP
Fold change in Shv
Unstim
Stim.
nsyb-GAL4>
repo-GAL4>
shv1;UAS-shv
E
Shv-eGFP
control
repo> Shv-RNAi
elav> Shv-RNAi
HRP/Shv-eGFP^extra
Fold change in Shv
control
repo> shv-RNAi
elav> shv-RNAi

Figure 6

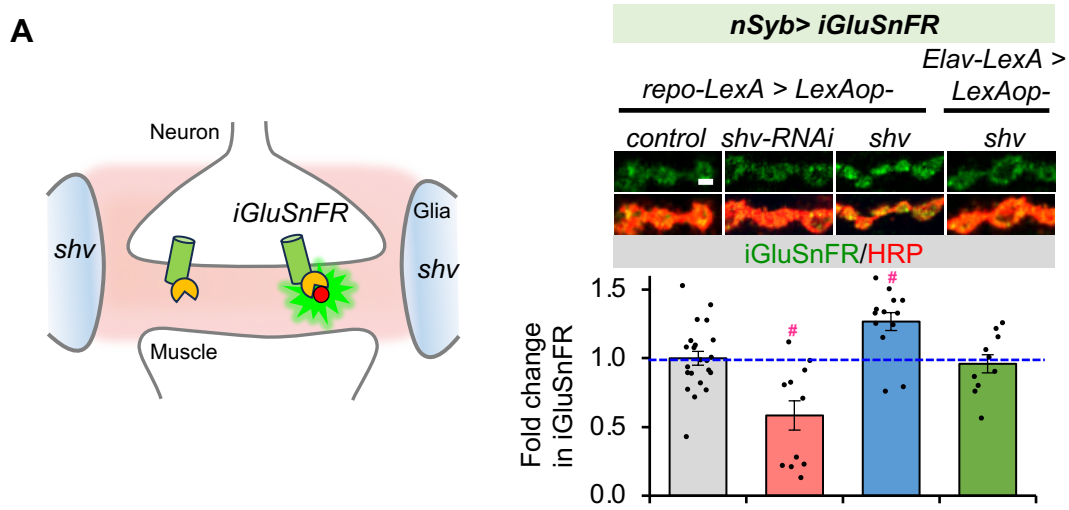
A
nSyb> iGluSnFR
repo-LexA > LexAop-
Elav-LexA > LexAop-
control
shv-RNAi
shv
shv
iGluSnFR/HRP
Neuron
iGluSnFR
Glia
shv
shv
Muscle
Fold change in iGluSnFR
1.5
1.0
0.5
0.0
#
#

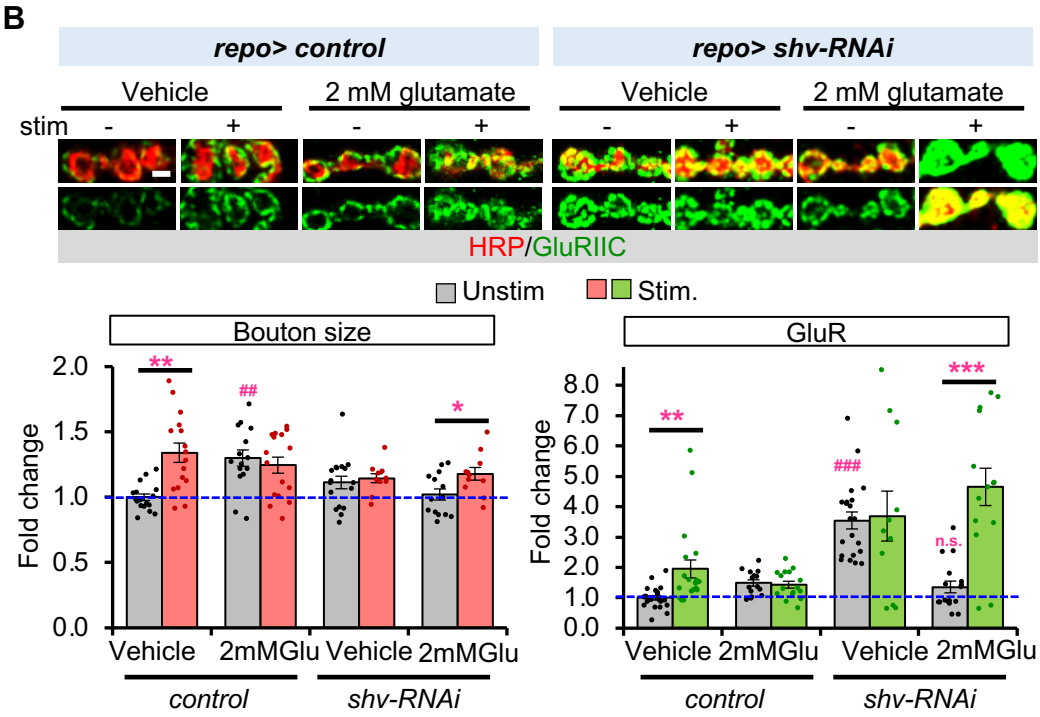
B
repo> control
repo> shv-RNAi
Vehicle
2 mM glutamate
Vehicle
2 mM glutamate
stim
-
+
-
+
-
+
-
+
HRP/GluRIIC
Unstim
Stim.
Bouton size
GluR
Fold change
2.0
1.5
1.0
0.5
0.0
**
##
*
8.0
7.0
6.0
5.0
4.0
3.0
2.0
1.0
0.0
**
###
n.s.
***
Vehicle
2mMGlu
Vehicle
2mMGlu
control
shv-RNAi

Figure 7

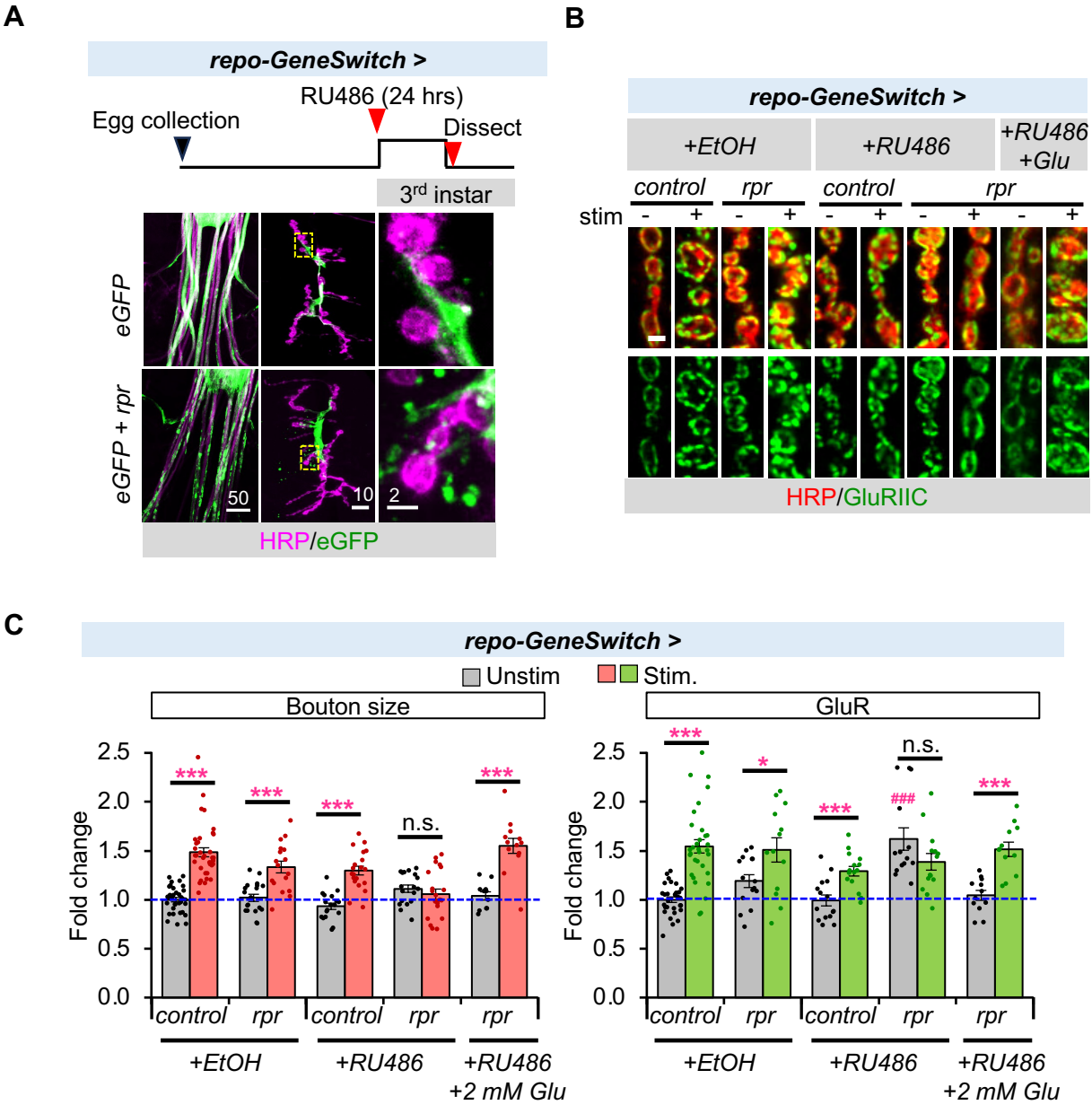
A
repo-GeneSwitch >
RU486 (24 hrs)
Egg collection
Dissect
3rd instar
eGFP
eGFP + rpr
50
10
2
HRP/eGFP
B
repo-GeneSwitch >
+EtOH
+RU486
+RU486 +Glu
control
rpr
control
rpr
stim
- + - + - + - + - +
HRP/GluRIIC
C
repo-GeneSwitch >
Unstim
Stim.
Bouton size
GluR
Fold change
2.5
2.0
1.5
1.0
0.5
0.0
***
n.s.
*
###
control
rpr
+EtOH
+RU486
+RU486 +2 mM Glu

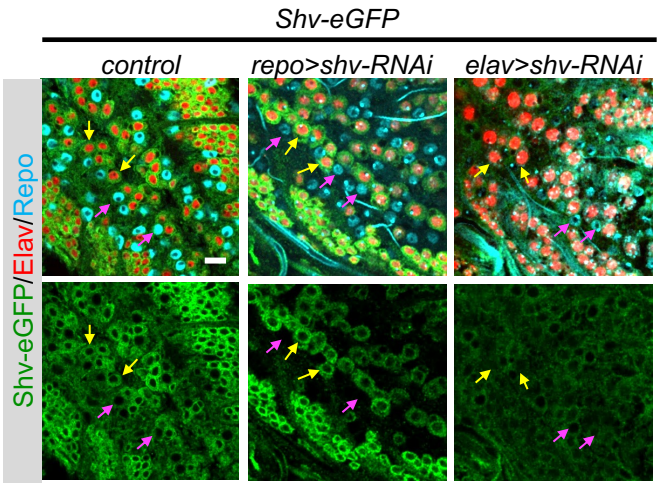

Supplementary Figure 1. Efficiency of *shv* knockdown by RNAi in neurons and glia. Staining of the larval brain confirms that the RNAi approach effectively reduces Shv-eGFP in the selective cell types. Yellow arrows highlight neurons (Elav positive), magenta arrows point to glial cells (Repo positive). Scale bar = 10 μm.

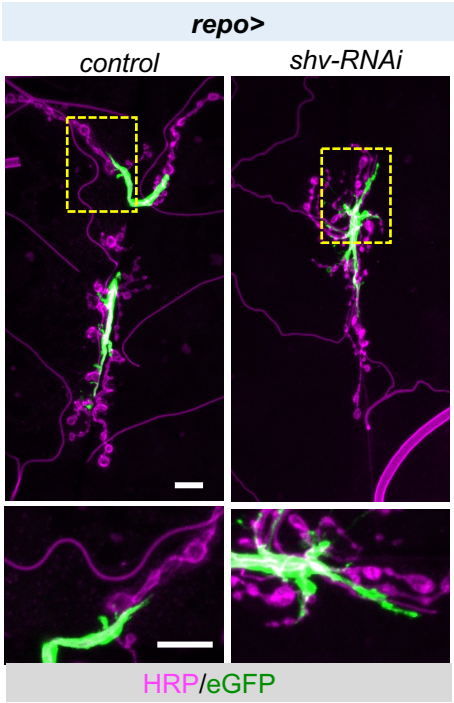

Supplementary Figure 2. Integrity of peripheral glial cell membranes. Representative images showing that knockdown of *shv* in glia does not alter the gross morphology of peripheral glia at the NMJ. Lower panels show magnified view of glia closely associating with proximal synaptic boutons. Scale bar = 10 μm.

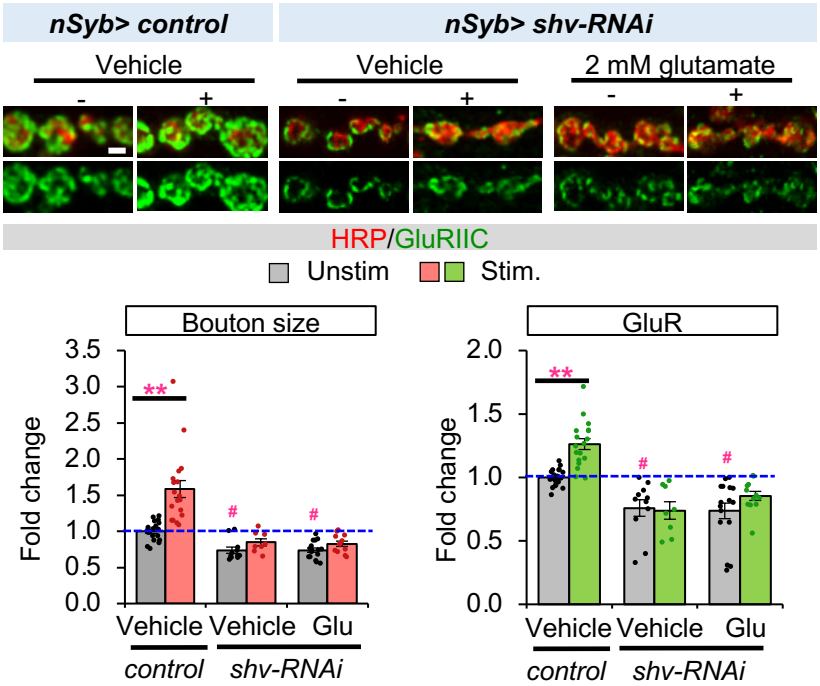

Supplementary Figure 3. Defective activity-induced synaptic remodeling caused by the loss of neuronal Shv is not rescued by incubation with 2 mM glutamate. Vehicle controls represent NMJs dissected in parallel and incubated with HL3 without 2 mM glutamate for the same length of time. Scale bar = 2 μm. All values are normalized to unstimulated control and presented as mean ± S.E.M. Control contains TRiP RNAi control vector driven by the neuronal driver. Statistics: One-way Anova followed by Tukey's multiple comparison test was used to compare between unstimulated control and unstimulated NMJs across genotypes. Student's t-test was used to compare between unstimulated and stimulated NMJs of the same genotype. # $p \leq 0.05$ when comparing unstimulated samples to unstimulated control. **$p \leq 0.01$ when comparing stimulated to unstimulated NMJs.